

## Synthesis of Bi<sub>2</sub>O<sub>3</sub>/BiVO<sub>4</sub> heterojunction with enhanced photocatalytic activity via single-step hydrothermal method

Chung-Hsin Wu<sup>a,\*</sup>, Chao-Yin Kuo<sup>b</sup>, Cheng-Di Dong<sup>c</sup>, Chiu-Wen Chen<sup>c</sup>, Yi-Li Lin<sup>d</sup>, Wei-Ming Chen<sup>a</sup>

<sup>a</sup>Department of Chemical and Materials Engineering, National Kaohsiung University of Science and Technology, 415 Chien Kung Road, Kaohsiung, Taiwan, Tel. +886-7-3814526; Fax: +886-7-3830674; emails: wuch@nkust.edu.tw (C.-H. Wu), x19921011@gmail.com (W.-M. Chen)

<sup>b</sup>Department of Safety, Health and Environmental Engineering, National Yunlin University of Science and Technology, Yunlin, Taiwan, Tel. +886-5-5347311; email: kuocyr@ms35.hinet.net

<sup>c</sup>Department of Marine Environmental Engineering, National Kaohsiung University of Science and Technology, Kaohsiung, Taiwan, Tel. +886-7-3617141; emails: cddong@nkust.edu.tw (C.-D. Dong), cwchen@nkust.edu.tw (C.-W. Chen)

<sup>d</sup>Department of Safety, Health and Environmental Engineering, National Kaohsiung University of Science and Technology, Kaohsiung, Taiwan, Tel. 886-7-6011000; email: yililin@nkust.edu.tw

Received 8 April 2019; Accepted 29 June 2019

### ABSTRACT

The single-step hydrothermal method was used to synthesize Bi<sub>2</sub>O<sub>3</sub>/BiVO<sub>4</sub> heterojunctions (BBVs) with various Bi<sub>2</sub>O<sub>3</sub>/BiVO<sub>4</sub> molar ratios. The surface characteristics of the prepared photocatalysts were analyzed by X-ray diffractometry (XRD), scanning electron microscopy, transmission electron microscopy, ultraviolet (UV)-visible-light (Vis.) spectrophotometry, surface area analysis, X-ray photoelectron spectroscopy and fluorescence spectrophotometry. C.I. Reactive Red 2 (RR2) was used as the parent compound to evaluate the photocatalytic activity of photocatalysts under UV and Vis. irradiation. The XRD peak intensity of BiVO<sub>4</sub> declined as the amount of Bi<sub>2</sub>O<sub>3</sub> in the BBVs increased. The surface areas of all BBVs exceeded those of Bi<sub>2</sub>O<sub>3</sub> and BiVO<sub>4</sub> and all of the samples exhibited strong absorption in the Vis. region. The optimal Bi<sub>2</sub>O<sub>3</sub>/BiVO<sub>4</sub> molar ratio was 0.25 and the corresponding photocatalyst was denoted as 0.25 BBV. The RR2 photodegradation rate constant of 0.25 BBV was 1.9 times that of BiVO<sub>4</sub> under UV irradiation, which was in turn 3.5 times that of BiVO<sub>4</sub> under Vis. irradiation. The improved photodegradation efficiency of BBVs is attributed to the effective separation of photo-generated carriers by the formed heterojunction. The results of a radical-trapping experiment revealed that the photo-generated holes and superoxide anion radicals were the primary reactive species in the BBV photocatalytic systems.

**Keywords:** BiVO<sub>4</sub>; Bi<sub>2</sub>O<sub>3</sub>; Heterojunction; Hydrothermal; Photocatalytic

### 1. Introduction

Semiconductor photocatalysis is regarded as a cost-effective and sustainable green chemical technique for eliminating organic pollutants from wastewater using solar energy. Bismuth-based oxide has attracted considerable

attention because of its strong response to visible-light (Vis.) and its lack of toxicity [1]. Bismuth vanadate (BiVO<sub>4</sub>) is a promising Vis.-driven photocatalyst with various advantages, such as low production cost, low toxicity, high photo-stability, resistance to photo-corrosion and a narrow band-gap with a good response to Vis. excitation [2]. Despite the

\* Corresponding author.

strong Vis. response, the photocatalytic ability of  $\text{BiVO}_4$  is poor owing to the poor migration of photo-generated electrons and holes [3]. Additionally, the rapid recombination of photo-produced electrons and holes in  $\text{BiVO}_4$  significantly reduces its photocatalytic reaction efficiency [4]. To solve this problem, the combination of  $\text{BiVO}_4$  with another semiconductor to form a heterojunction has been proposed, with the goal of improving electron-hole pair separation and interfacial charge transfer efficiency, to promote photocatalytic activity.

A series of  $\text{BiVO}_4$ -based heterojunction photocatalysts with various morphologies have been reported. They include  $\text{TiO}_2/\text{BiVO}_4$  [5–7],  $\text{Cu}_2\text{O}/\text{BiVO}_4$  [8–10],  $\text{Bi}_2\text{WO}_6/\text{BiVO}_4$  [11–14],  $\text{Bi}_2\text{O}_3/\text{BiVO}_4$  [4,15–19],  $\text{BiFeWO}_6/\text{BiVO}_4$  [20],  $\text{WO}_3/\text{BiVO}_4$  [21];  $\text{InVO}_4/\text{BiVO}_4$  [22];  $\text{CuS}/\text{BiVO}_4$  [23] and  $\text{BiOCl}/\text{BiVO}_4$  [24,25], which are prepared by various methods and exhibit excellent photocatalytic performance. The coupling of  $\text{BiVO}_4$  with other semiconductors is an efficient approach to promote the charge separation reaction and slow the recombination of photo-generated charge carriers.

The optimal 20%  $\text{TiO}_2/\text{BiVO}_4$  composite exhibits better photocatalytic performance than  $\text{BiVO}_4$ . The higher photocatalytic activity of the  $\text{TiO}_2/\text{BiVO}_4$  is attributable to the increased separation efficiency of photo-induced charge carriers [5]. The optimized  $\text{Cu}_2\text{O}/\text{BiVO}_4$  composite exhibits greater photocatalytic activity than  $\text{BiVO}_4$ . Its superior photocatalytic performance may arise from the successful charge separation of electron-hole pairs by the formed heterojunction between  $\text{Cu}_2\text{O}/\text{BiVO}_4$  nanoparticles [8–10]. The improved photocatalytic activity of  $\text{Bi}_2\text{WO}_6/\text{BiVO}_4$  is due to the formation of the heterojunction by the matching of the energy levels of bands, which increases the separation efficiency of photo-induced charge carriers, favoring the degradation of organic contaminants [11,12,14].

Bismuth oxide ( $\text{Bi}_2\text{O}_3$ ) is an ideal Vis.-driven photocatalyst because of its bandgap (2.8 eV), the high oxidation power of its holes in the valance band (VB), nontoxicity, and stability. However, it has a low photocatalytic activity because of the rapid recombination of photo-generated electron-hole pairs [26,27].  $\text{Bi}_2\text{O}_3$ -based heterojunctions, which enable photocatalysts to use more Vis. and effectively suppress photo-generated electron-hole recombination have been synthesized to improve the photoactivity of  $\text{BiVO}_4$ . Li and Yan [4] prepared  $\text{Bi}_2\text{O}_3/\text{BiVO}_4$  heterojunctions (BBVs) by directly mixing two semiconductors and found that  $\text{Bi}_2\text{O}_3$  (50 wt.)/ $\text{BiVO}_4$  exhibited the highest photocatalytic activity. They suggested that the mixture reduced the rate of recombination of photo-generated electron-hole pairs that in pure  $\text{Bi}_2\text{O}_3$  or  $\text{BiVO}_4$  and thereby improved its photocatalytic activity. Lee et al. [19] provided evidence of the feasibility of using  $\text{BiVO}_4/\text{Bi}_2\text{O}_3$  as a photocatalyst in the removal of polychlorinated dibenzo-p-dioxins and dibenzofurans from soil.  $\text{BiVO}_4/\text{Bi}_2\text{O}_3$  with 20%  $\text{BiVO}_4$  content by mass ( $\text{BiVO}_4/\text{Bi}_2\text{O}_3$  molar ratio = 0.360) performed best in their work. Reductive reactions occur on  $\text{BiVO}_4$ , while oxidative reactions occur on  $\text{Bi}_2\text{O}_3$  [19]. Mao et al. [16] used a solvothermal method followed by an annealing process to synthesize porous BBVs and found that the photocatalytic activity of BBVs was more than 48 times that of a mixture of  $\text{BiVO}_4$  and  $\text{Bi}_2\text{O}_3$ , and 192 and 160 times those of  $\text{BiVO}_4$  and  $\text{Bi}_2\text{O}_3$ , respectively. Sun et al. [18] prepared BBVs with an effective *p-n* heterojunction via a hydrothermal route to improve upon the photocatalytic performance of  $\text{BiVO}_4$ .

The dramatic enhancement of photoactivity is attributable to the high separation efficiency of electron-hole pairs in BBVs [16,18]. Qiu et al. [17] used chemical deposition to synthesize BBVs, whose photocatalytic activity was 1.5 times that of a mixture of  $\text{BiVO}_4$  and  $\text{Bi}_2\text{O}_3$ . Chen et al. [15] synthesized BBVs using a single-step mixed solvothermal method and an L-lysine template. The heterojunctions that formed between  $\text{BiVO}_4$  and  $\text{Bi}_2\text{O}_3$  promoted the separation of photo-generated electron-hole pairs, and their hollow porous structure enabled the efficient harvesting of solar light.

The formation of a heterojunction interface between two semiconductors with matching energy levels can facilitate interfacial charge transfer and improve the separation of photo-induced charges in a semiconductor composite. The *p-n* heterojunction is an interesting and special heterostructure owing to its internal electric field at the heterojunction interface, and its structure improves the separation of photo-generated electron-hole pairs, increasing photocatalytic activity [13,16–19,23]. Researchers have not yet used a single-step hydrothermal method to synthesize BBVs with various  $\text{Bi}_2\text{O}_3/\text{BiVO}_4$  molar ratios and compared their photocatalytic activities. The goals of the present work are (i) to synthesize BBVs with different  $\text{Bi}_2\text{O}_3/\text{BiVO}_4$  molar ratios, (ii) to measure the surface characteristics and compare the photocatalytic activities of the prepared BBVs, and (iii) to determine the reusability and the active reaction species of BBVs at the optimal  $\text{Bi}_2\text{O}_3/\text{BiVO}_4$  molar ratio.

## 2. Materials and methods

### 2.1. Materials

All reagents were analytical-grade and used as received without further purification. Deionized water (D.I. water) was used throughout this study. Bismuth (III) nitrate ( $\text{Bi}(\text{NO}_3)_3 \cdot 5\text{H}_2\text{O}$ ), ammonium metavanadate ( $\text{NH}_4\text{VO}_3$ ), trisodium citrate (TCD,  $\text{Na}_3\text{C}_6\text{H}_5\text{O}_7 \cdot 2\text{H}_2\text{O}$ ), NaOH,  $\text{HNO}_3$ , disodium ethylenediamine tetraacetate ( $\text{EDTA-2Na}$ ,  $\text{C}_{10}\text{H}_{14}\text{N}_2\text{O}_8\text{Na}_2 \cdot 2\text{H}_2\text{O}$ ) and potassium chromate ( $\text{K}_2\text{CrO}_4$ ) were all purchased from Katayama (Japan). RR2 ( $\text{C}_{19}\text{H}_{10}\text{Cl}_2\text{N}_6\text{Na}_2\text{O}_7\text{S}_2$ ) and isopropanol (IPA) were obtained from Sigma Aldrich (USA) and J.T. Baker (USA), respectively.

### 2.2. Synthesis of photocatalysts

The BBVs were prepared using a single-step hydrothermal process, the details of which are as follows. 0.7019 g of  $\text{NH}_4\text{VO}_3$  was dissolved in 60 mL 2 M NaOH to yield solution A. The desired amount of  $\text{Bi}(\text{NO}_3)_3 \cdot 5\text{H}_2\text{O}$  was added to 60 mL 2 M  $\text{HNO}_3$  to form solution B. 0.5294 g of TCD was dissolved in 20 mL D.I. water to form solution C. The obtained mixtures were adjusted to pH 1 by adding 10 M NaOH or  $\text{HNO}_3$  and stirred (600 rpm) for 30 min. Each was sealed in a 200 mL Teflon-lined stainless steel autoclave and heated at 473 K under self-generated pressure for 12 h; it was then allowed to cool naturally to room temperature. The precipitates were collected by filtration and washed using 50 mL 95% ethanol and 100 mL D.I. water to remove any residual impurities. The samples were finally dried in air at 333 K for 24 h. A series of BBVs were prepared by changing the Bi/V mole ratios of the starting materials, and the photocatalytic

efficiencies of the BBVs were compared with those of only  $\text{Bi}_2\text{O}_3$  or  $\text{BiVO}_4$ . Five Bi/V molar ratios (1.2, 1.5, 2.0, 2.5 and 3.0) were used in the syntheses, yielding 0.1BBV, 0.25BBV, 0.5BBV, 0.75BBV and 1BBV, respectively. When no  $\text{NH}_4\text{VO}_3$  or TCD was added, the obtained powder was  $\text{Bi}_2\text{O}_3$ .  $\text{BiVO}_4$  was prepared using a Bi/V molar ratio of unity. The experimental conditions and procedures for synthesizing  $\text{Bi}_2\text{O}_3$  and  $\text{BiVO}_4$  were the same as those for generating BBVs.

### 2.3. Surface analyses of photocatalysts

The crystalline structures of the photocatalysts were analyzed using X-ray diffraction (XRD) with Cu-K $\alpha$  radiation (Bruker D8 SSS, Germany) over a  $2\theta$  range of  $20^\circ$ – $80^\circ$ . The accelerating voltage and the applied current were set to 40 kV and 40 mA, respectively. The morphologies and microstructures of the samples were observed using a scanning electron microscope (SEM, JEOL 6330 TF, Japan) and transmission electron microscope (TEM, JEOL 3010, Japan). The bandgaps were calculated from the diffuse reflectance ultraviolet (UV)-Vis. spectra of photocatalysts, which were obtained using a UV-Vis spectrophotometer (JAS.CO-V670, Japan).  $\text{N}_2$  adsorption-desorption isotherms were obtained at 77 K on a Micrometrics ASAP 2020 surface area analyzer (USA). The Brunauer-Emmett-Teller (BET) method was used to calculate the specific surface areas from adsorption data. X-ray photoelectron spectroscopy (XPS) measurements were made at room temperature using a PHI 5000 Versal Probe XPS (USA). The binding energies were calibrated against  $\text{C}_{1s}$  at 284.6 eV. The photoluminescence (PL) spectra were measured using an excitation wavelength of 325 nm and a Hitachi F-4500 fluorescence spectrophotometer (Japan).

### 2.4. Photocatalysis experiments

The photocatalyst dosage, RR2 concentration and temperature in all of the experiments were 0.5 g/L, 20 mg/L

and 298 K, respectively. The solution pH was 3 in all experiments except those conducted to determine the effects of pH. Photocatalysis experiments were performed in a 3 L glass reactor. A 400 W Xe lamp ( $200 \text{ nm} < \text{wavelength} < 700 \text{ nm}$ , UniVex BT-580, Taiwan) was used to provide UV radiation and the intensity of the light from the lamp was  $30.3 \text{ mW/cm}^2$ . A quartz appliance that was filled with 2 M  $\text{NaNO}_2$  solution was placed on top of the reactor to cut the UV and to provide Vis. [28]. Adsorption experiments were performed in darkness. The reaction medium was stirred continuously at 300 rpm and aerated with air to maintain a suspension. Following sampling at specific intervals, solids were separated by filtration through a  $0.22 \mu\text{m}$  filter (Millipore, USA), and the RR2 that remained in the filtrate was analyzed by measuring its absorbance at 538 nm using a spectrophotometer (Hitachi U-5100, Japan). The stability and reusability of 0.25BBV were examined under the same conditions as in the photocatalytic experiments. At the end of each cycle, the recovered 0.25BBV was centrifuged and dried at 333 K for 24 h. Then, the powder was used in the next cycle. The 0.25BBV was re-dispersed into a fresh RR2 solution and recycled three times. To detect the active species that were responsible for photocatalytic reactivity, trapping experiments were conducted. In a process similar to that in the photocatalysis experiment, scavengers  $\text{K}_2\text{CrO}_4$ , EDTA-2Na and IPA were introduced into the RR2 solution before the photocatalyst was added; these were scavengers of superoxide anion radicals ( $\cdot\text{O}_2^-$ ) [29], holes ( $\text{h}^+$ ) [30,31] and hydroxyl radicals ( $\cdot\text{OH}$ ) [30,31], respectively. The experiments were conducted in triplicate and mean values reported.

## 3. Results and discussion

### 3.1. Surface characteristics of $\text{Bi}_2\text{O}_3$ , $\text{BiVO}_4$ and BBVs

To determine the phase structures of  $\text{Bi}_2\text{O}_3$ ,  $\text{BiVO}_4$  and BBV powders, their XRD patterns were measured (Fig. 1).

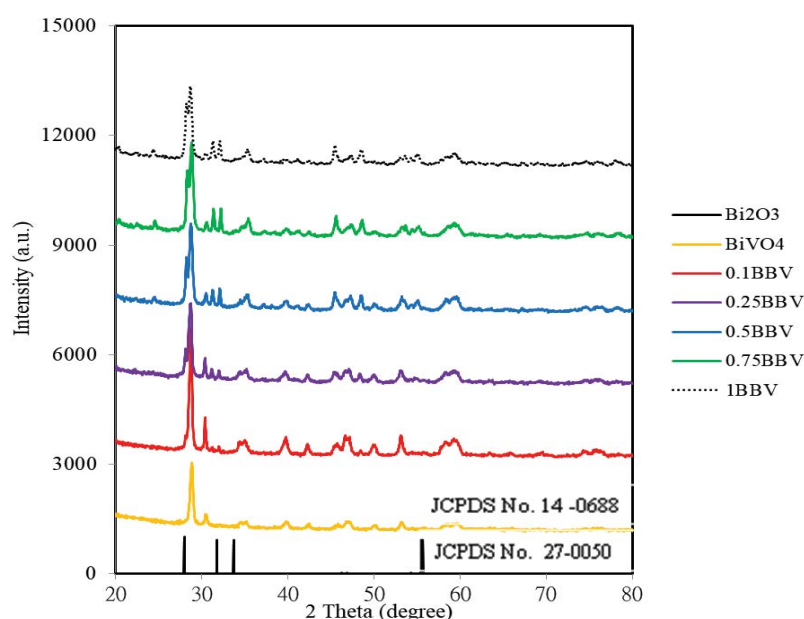


Fig. 1. XRD patterns of  $\text{Bi}_2\text{O}_3$ ,  $\text{BiVO}_4$  and BBVs.

The patterns in Fig. 1 included sharp peaks, indicating that  $\text{Bi}_2\text{O}_3$ ,  $\text{BiVO}_4$  and BBVs that were synthesized by the hydrothermal process had a high degree of crystallinity, and the BBVs had peaks that were characteristic of the obtained  $\text{Bi}_2\text{O}_3$  and  $\text{BiVO}_4$ . The obtained  $\text{Bi}_2\text{O}_3$  and  $\text{BiVO}_4$  were readily indexed to the monoclinic phase of  $\text{BiVO}_4$  (JCPDS No. 14-0688) and the tetragonal phase of  $\beta\text{-Bi}_2\text{O}_3$  (JCPDS No. 27-0050), respectively. The peak intensity of  $\text{BiVO}_4$  decreased as the amount of  $\text{Bi}_2\text{O}_3$  in the BBVs increased. Notably, no signal other than those of  $\text{Bi}_2\text{O}_3$  and  $\text{BiVO}_4$  was obtained in the diffraction patterns, revealing that  $\text{Bi}_2\text{O}_3$  and  $\text{BiVO}_4$  did not chemically react. The XRD results reveal the complete transformation of BBVs from precursors, as was also observed by Mao et al. [16].

The morphologies of the synthesized materials were ascertained using SEM and TEM. Figs. 2a–c show SEM images of  $\text{Bi}_2\text{O}_3$ ,  $\text{BiVO}_4$  and 0.25BBV, respectively.  $\text{Bi}_2\text{O}_3$  comprised irregular plates with smooth surface structures (Fig. 2a).  $\text{BiVO}_4$  was in the form of aggregated lumps. Clearly, the  $\text{BiVO}_4$  mainly consisted of small granules (Fig. 2b), and had conglomerated more than the  $\text{Bi}_2\text{O}_3$  particles (Fig. 2a).

The surface morphology of 0.25BBV revealed smaller nanoparticles of  $\text{BiVO}_4$  that were distributed on the particles of  $\text{Bi}_2\text{O}_3$  (Fig. 2c). Figs. 3a–c display TEM images of  $\text{Bi}_2\text{O}_3$ ,  $\text{BiVO}_4$  and 0.25BBV, respectively, which show that the samples comprised many agglomerates of primary nanoparticles. Fig. 3c demonstrates that many nanocrystals were homogeneously dispersed and embedded in sheets of 0.25BBV. These observations reveal close contact between  $\text{Bi}_2\text{O}_3$  and  $\text{BiVO}_4$  in 0.25BBV. Both  $\text{BiVO}_4$  and 0.25BBV were peanut-like structures, similar to those found by Chen et al. [15].

The BET surface areas of  $\text{Bi}_2\text{O}_3$ ,  $\text{BiVO}_4$ , 0.1BBV, 0.25BBV, 0.5BBV, 0.75BBV and 1BBV were 0.2, 2.9, 6.3, 3.8, 11.0, 14.8 and 7.4  $\text{m}^2/\text{g}$ , respectively. The BET surface areas of the BBVs all exceeded those of  $\text{Bi}_2\text{O}_3$  and  $\text{BiVO}_4$  (Table 1). Based on the BET investigation, the BBVs had larger surface areas than  $\text{Bi}_2\text{O}_3$  and  $\text{BiVO}_4$ , providing more active sites, favoring photocatalytic activity.

The absorption of Vis. is important in evaluating Vis.-driven photocatalytic activity. Fig. 4 presents UV-Vis diffuse reflectance spectra of  $\text{Bi}_2\text{O}_3$ ,  $\text{BiVO}_4$  and BBVs powders. All of the samples except for  $\text{Bi}_2\text{O}_3$  exhibit strong absorption

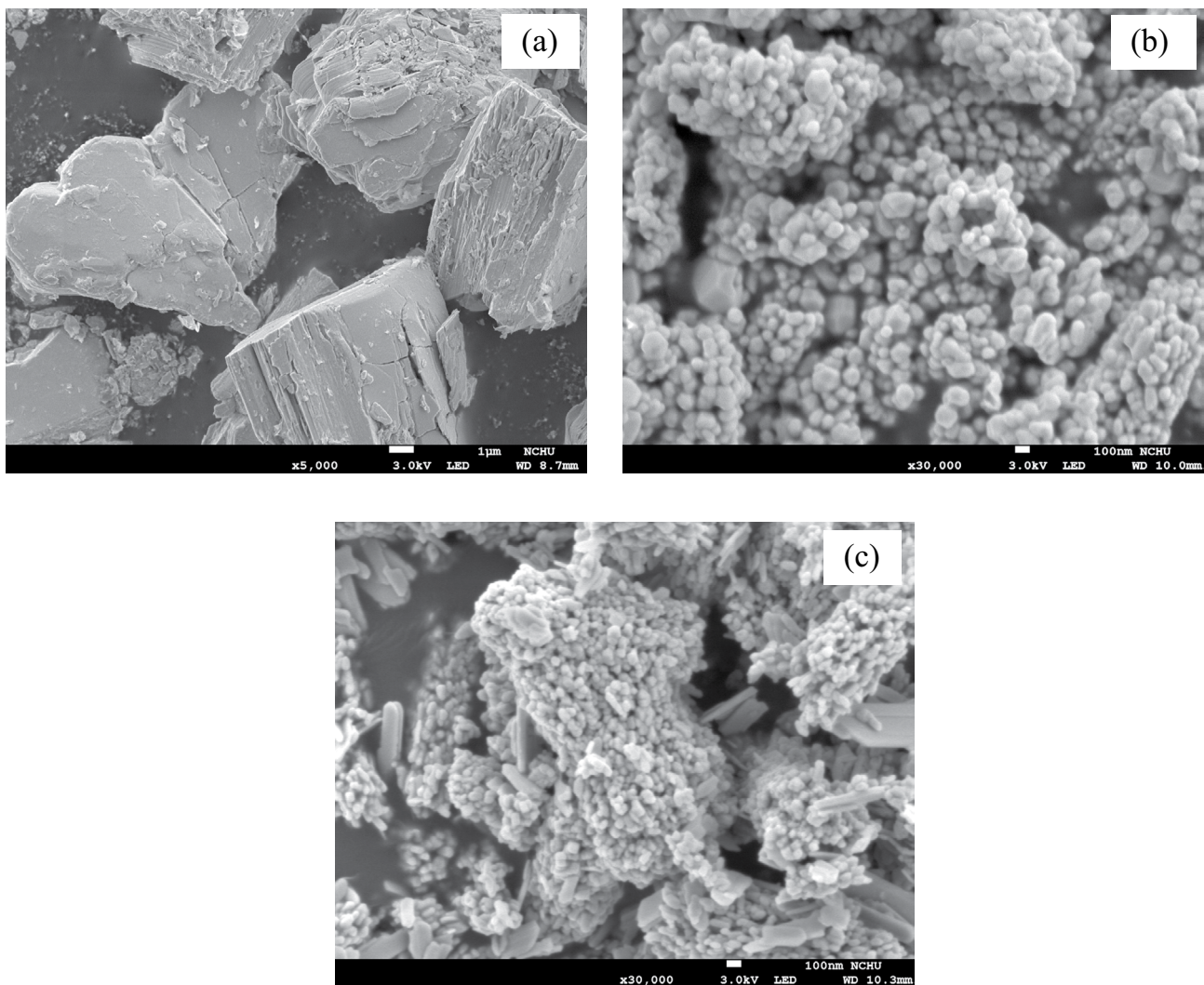


Fig. 2. SEM image of photocatalyst (a)  $\text{Bi}_2\text{O}_3$ , (b)  $\text{BiVO}_4$  and (c) 0.25BBV.

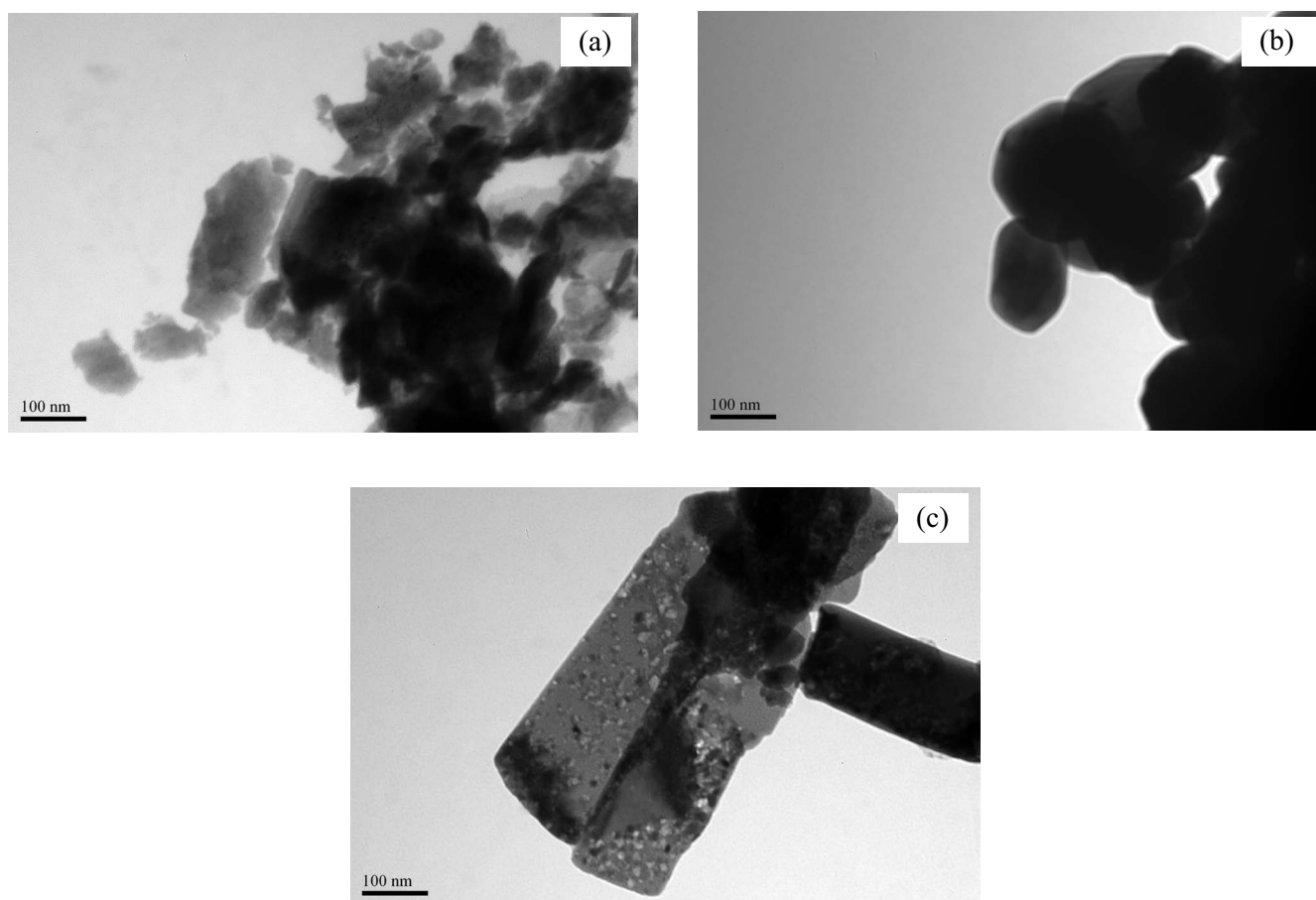


Fig. 3. TEM image of photocatalyst (a)  $\text{Bi}_2\text{O}_3$ , (b)  $\text{BiVO}_4$  and (c) 0.25BBV.

Table 1  
Surface characteristics of prepared photocatalysts

Catalysts	BET surface area ( $\text{m}^2/\text{g}$ )	Bandgap (eV)	UV		Vis.	
			$k$ ( $\text{min}^{-1}$ )	$R^2$	$k$ ( $\text{min}^{-1}$ )	$R^2$
$\text{BiVO}_4$	2.9	2.44	0.0115	0.999	0.004	0.986
$\text{Bi}_2\text{O}_3$	0.2	2.89	–	–	–	–
0.1BBV	6.7	2.48	0.0197	0.980	0.013	0.969
0.25BBV	3.8	2.49	0.0218	0.988	0.014	0.971
0.5BBV	11.0	2.51	0.0273	0.993	0.013	0.998
0.75BBV	14.8	2.51	0.0173	0.991	0.016	0.990
1BBV	7.4	2.51	0.0134	0.987	0.008	0.988

in the Vis.-region. The calculated bandgap is estimated from  $l = 1,240/E_g$ , where  $l$  and  $E_g$  denote the absorption band threshold wavelength (nm) and bandgap (eV), respectively. The absorption band thresholds of  $\text{Bi}_2\text{O}_3$ ,  $\text{BiVO}_4$ , 0.1BBV, 0.25BBV, 0.5BBV, 0.75BBV and 1BBV are approximately 435, 510, 499, 500, 500 and 500 nm, and the bandgaps are estimated to be 2.89, 2.44, 2.48, 2.49, 2.51, 2.51 and 2.51 eV, respectively (Table 1). The obtained BBVs did not vary much in their capacity to absorb light. The absorption edge of BBVs exhibits a tiny blue-shift relative to that of  $\text{BiVO}_4$ ,

owing to the incorporation of  $\text{Bi}_2\text{O}_3$ . This finding was also obtained by Shi et al. [1].

PL spectral analysis is employed to examine the migration, transfer and recombination rate of charge carriers in photocatalysts. Increasing the separation and transfer rates of electron-hole pairs and reducing the photo-generated charge carrier recombination rate can significantly improve the photocatalytic performance of photocatalysts. Generally, a lower PL intensity reflects a lower rate of recombination of electron-hole pairs, resulting in better photocatalytic

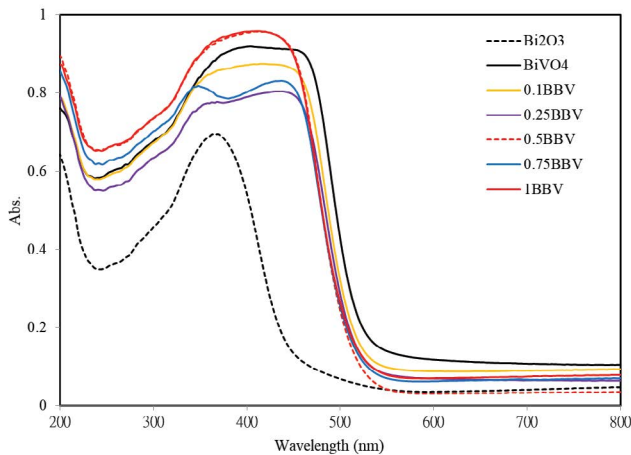


Fig. 4. UV-Vis absorption spectra of  $\text{Bi}_2\text{O}_3$ ,  $\text{BiVO}_4$  and BBVs.

performance. Fig. 5 shows the PL spectra of  $\text{Bi}_2\text{O}_3$ ,  $\text{BiVO}_4$  and BBVs. The PL intensities of 0.25BBV, 0.5BBV and 0.75BBV were lower than those of  $\text{Bi}_2\text{O}_3$  and  $\text{BiVO}_4$  (Fig. 5), indicating that the 0.25BBV, 0.5BBV and 0.75BBV exhibited higher photo-induced charge separation efficiencies than the pure samples.

The surface compositions of 0.25BBV and the chemical states of its elements were analyzed by XPS (Fig. 6). In the high-resolution spectrum of  $\text{Bi}_{4f}$  (Fig. 6a), two characteristic peaks at 164.0 and 158.5 eV that arose from the  $4f_{5/2}$  and  $4f_{7/2}$  orbitals, respectively [15,18,32,33], are assigned to the +3 bismuth state, suggesting that the bismuth ions in the 0.25BBV composite were in the trivalent state. The characteristic spin-orbit splitting of the  $\text{V}_{2p_{3/2}}$  and  $\text{V}_{2p_{1/2}}$  signals was observed at approximately 516.5 and 524.0 eV, respectively, corresponding to  $\text{V}^{5+}$  in  $\text{BiVO}_4$  (Fig. 6b) [15,18,33,34]. The asymmetrical  $\text{O}_{1s}$  signal is fitted to three bands at 529.6, 530.3 and 532.0 eV (Fig. 6c). The peaks at 529.6 and 530.0 eV correspond to the Bi-O bond in  $\text{Bi}_2\text{O}_3$  and the oxygen species in the lattice ( $\text{O}^{2-}$ ) in  $\text{BiVO}_4$ , respectively. The band at 532.0 eV is attributed to surface-adsorbed oxygen species of hydroxyl-like groups or the O-defect oxide [18,35,36].

The elemental ratio in the surface region of the sample was obtained by XPS analysis. Table 2 presents the Bi-O/V-O ratios that are associated with the  $\text{O}_{1s}$  signals in the XPS spectra of the BBVs. The Bi-O/V-O elemental ratios of 0.1BBV, 0.25BBV, 0.5BBV, 0.75BBV and 1BBV were found to be 1.18, 1.49, 1.91, 2.37 and 2.97, respectively. The quantitative atomic analysis of Bi-O/V-O in BBVs is almost the same as the dose of  $\text{Bi}_2\text{O}_3$  that was added to  $\text{BiVO}_4$ .

### 3.2. Photocatalytic activity of $\text{Bi}_2\text{O}_3$ , $\text{BiVO}_4$ and BBVs

Figs. 7a–c plot the removal of RR2 by adsorption, Vis. photocatalysis and UV photocatalysis, respectively. After 180 min of reaction, the percentages of RR2 that were adsorbed by  $\text{Bi}_2\text{O}_3$ ,  $\text{BiVO}_4$ , 0.1BBV, 0.25BBV, 0.5BBV, 0.75BBV and 1BBV were 2%, 15%, 24%, 21%, 35%, 40% and 33%, respectively (Fig. 7a). After 180 min of reaction, the percentages of RR2 that had been removed by  $\text{Bi}_2\text{O}_3$ ,  $\text{BiVO}_4$ , 0.1BBV, 0.25BBV, 0.5BBV, 0.75BBV and 1BBV with Vis. photocatalysis were 3%, 56%, 87%, 87%, 89%, 92% and 79%, respectively

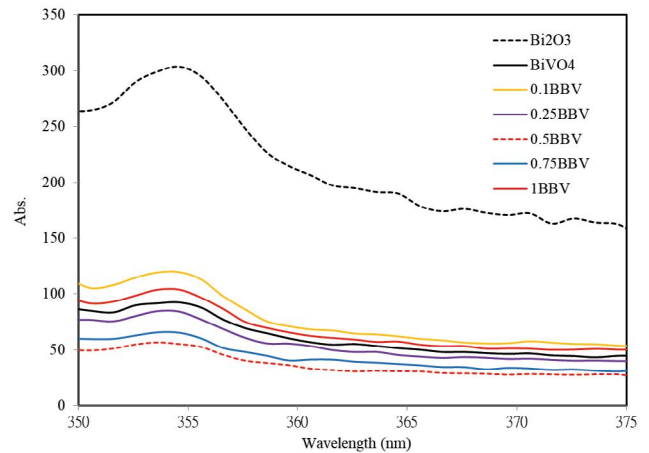


Fig. 5. PL spectra of  $\text{Bi}_2\text{O}_3$ ,  $\text{BiVO}_4$  and BBVs.

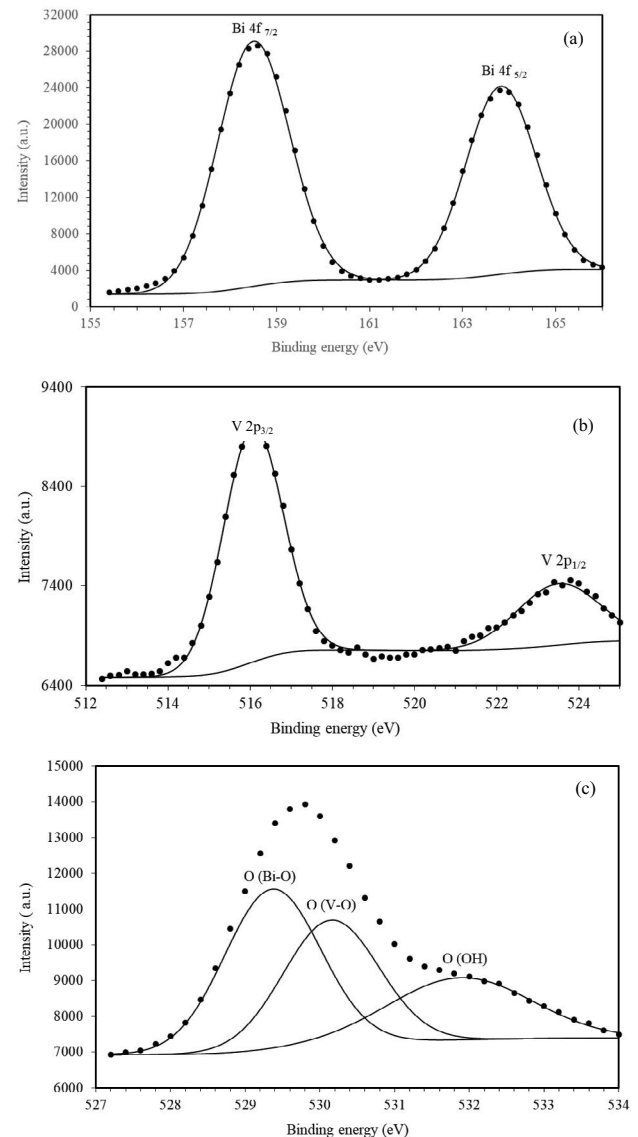


Fig. 6. XPS spectra of 0.25BBV (a)  $\text{Bi}_{4f}$ , (b)  $\text{V}_{2p}$  and (c)  $\text{O}_{1s}$ .

Table 2  
Bi-O/V-O ratios determined from O<sub>1s</sub> signal in XPS spectra of BBVs

	BiVO <sub>4</sub>	Bi <sub>2</sub> O <sub>3</sub>	0.1BBV	0.25BBV	0.5BBV	0.75BBV	1BBV
Bi–O	43%	46%	44%	46%	49%	53%	57%
V–O	44%	0%	37%	31%	26%	22%	19%
–OH	13%	54%	19%	23%	25%	25%	24%
Bi–O/V–O	0.97		1.18	1.49	1.91	2.37	2.97
Actual ratio			0.09BBV	0.245BBV	0.455BBV	0.685BBV	0.985BBV

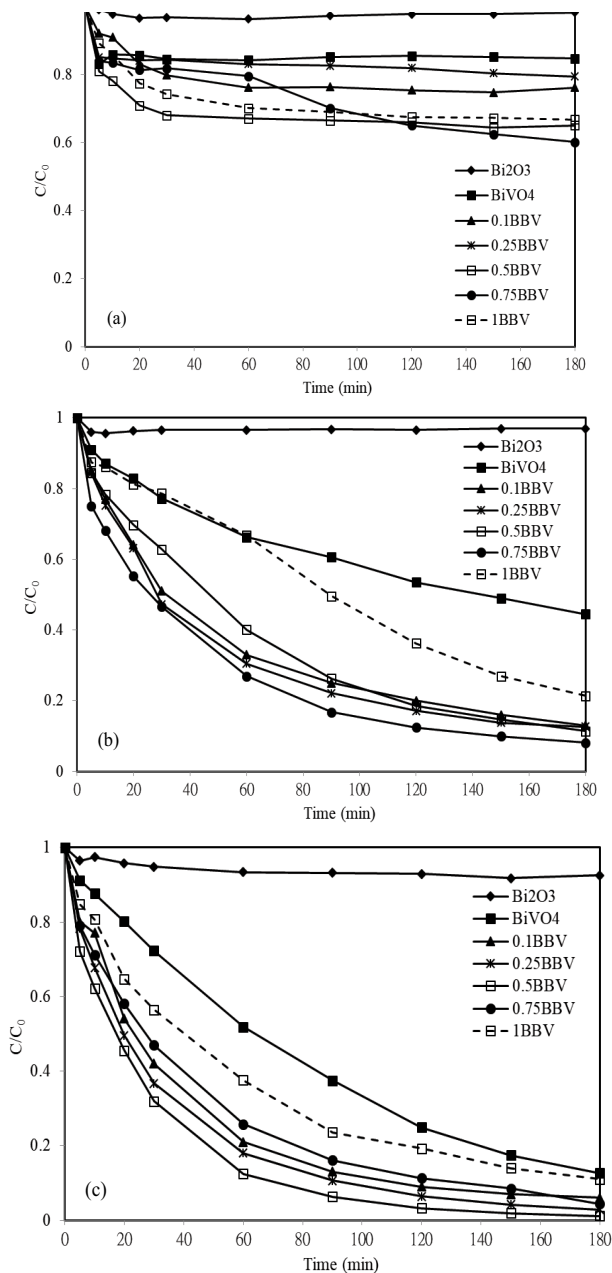


Fig. 7. Comparisons of decolorization of RR2 by Bi<sub>2</sub>O<sub>3</sub>, BiVO<sub>4</sub> and BBVs by (a) adsorption, (b) Vis. Photocatalysis, and (c) UV photocatalysis ([RR2] = 20 mg/L, pH = 3, [photocatalyst] = 0.5 g/L).

(Fig. 7b), and with UV photocatalysis were 8%, 87%, 94%, 97%, 99%, 96% and 89%, respectively (Fig. 7c). The photoactivity of Bi<sub>2</sub>O<sub>3</sub> was low despite its ability to absorb Vis.. The high recombination rate of photo-excited electrons and holes in Bi<sub>2</sub>O<sub>3</sub> significantly reduced the efficiency of the photocatalysis. With respect to the net efficiency of RR2 removal by adsorption and photocatalysis, 0.25BBV exhibited the highest photocatalytic activity under both UV and Vis. irradiation.

The kinetics of the removal of RR2 are well described by the pseudo-first-order equation  $\ln(C_0/C) = k_t$ , where  $k$  is the rate constant;  $C_0$  is the initial concentration of RR2;  $C$  is the concentration of RR2 after irradiation, and  $t$  is the irradiation time [1,17,19,20,23,25,33]. All kinetic data agree closely with the pseudo-first-order equation because the R<sup>2</sup> values exceed 0.97 (Table 1). In this investigation, the  $k$  values of 0.25BBV under UV and Vis. irradiation were 0.0218 and 0.014 min<sup>-1</sup>, respectively (Table 1). The  $k$  value of 0.25BBV was 1.9 times that of BiVO<sub>4</sub> under UV irradiation, which was 3.5 times larger than BiVO<sub>4</sub> that under Vis. irradiation. These experimental results revealed that the formation of BBVs greatly increased the photocatalytic activity of BiVO<sub>4</sub>. The  $k$  values followed the order BBVs > BiVO<sub>4</sub> > Bi<sub>2</sub>O<sub>3</sub>, which was also obtained by Shi et al. [1]. Factors other than photo-absorption are also important in increasing the photocatalytic efficiency of photocatalysts; they include the separation efficiency of photo-generated electron-hole pairs and the number of effectively active sites for photocatalysis. The enhanced photoactivity of BBVs can be explained as follows. The larger specific surface area of BBVs than of Bi<sub>2</sub>O<sub>3</sub> (0.2 m<sup>2</sup>/g) and BiVO<sub>4</sub> (2.9 m<sup>2</sup>/g) (Table 1) results in greater contact between BBVs and RR2 and improves the separation efficiency of photo-induced electron-hole pairs. Lee et al. [19] indicated that the electrons in the conduction band (CB) of Bi<sub>2</sub>O<sub>3</sub> easily moved to that of BiVO<sub>4</sub> while the holes were easily transferred from the VB of BiVO<sub>4</sub> to Bi<sub>2</sub>O<sub>3</sub> owing to the inherent band relationship.

Fig. 8 plots the effects of light sources and pH on the decolorization of RR2 in BiVO<sub>4</sub> and 0.25BBV systems. The pH of the solution affects the adsorption and dissociation of RR2, the surface charge of the photocatalyst, and the oxidation potential of the photocatalyst. After 60 min of reaction, the photocatalytic removal of RR2 by 0.25BBV under UV irradiation at pH 3 and 9 was 97% and 43%, respectively, and that by BiVO<sub>4</sub> was 87% and 13%, respectively. RR2 is an anionic dye in solution. The repulsive force between the photocatalyst and RR2 was stronger at pH 9 than at pH 3 so the photocatalytic efficiency at pH 3 exceeded that at pH 9. Comparisons

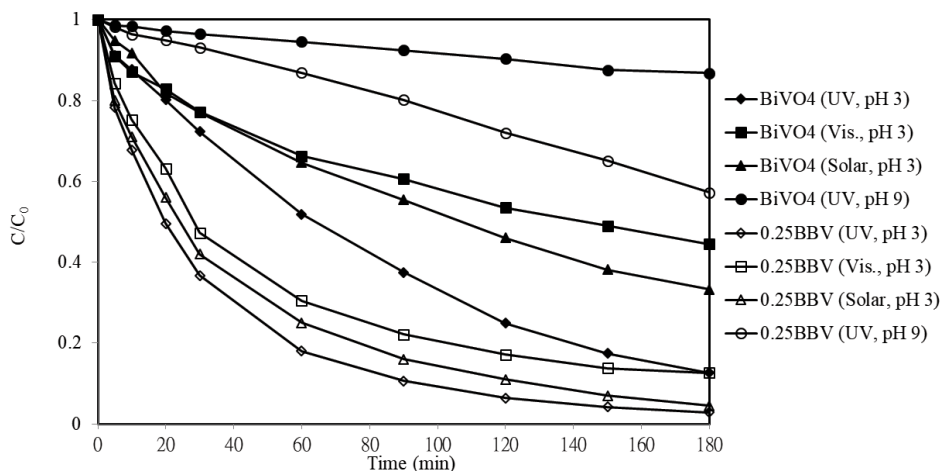


Fig. 8. Effects of light sources and pH on RR2 decolorization in BiVO<sub>4</sub> and 0.25BBV systems ([RR2] = 20 mg/L, [photocatalyst] = 0.5 g/L).

of BiVO<sub>4</sub> and 0.25BBV revealed that the *k* values followed the orders UV > Solar > Vis. and 0.25BBV > BiVO<sub>4</sub>.

Recyclability tests were conducted to assess the reusability of 0.25BBV for the photodegradation of RR2. The RR2 photodegradation efficiency of 0.25BBV after one, two and three cycles under UV irradiation was 97%, 97% and 95%, respectively, and after one, two and three cycles under Vis. irradiation was 87%, 86% and 84% (Fig. 9). As shown in Fig. 9, 0.25BBV was stable, and no loss of photocatalytic activity occurred in the three-cycle test. The experimental results suggest that 0.25BBV had good reusability and did not undergo photo-corrosion under UV or Vis. irradiation.

### 3.3. Mechanism of enhancement of photocatalytic activity

As expected,  $\cdot\text{O}_2^-$ ,  $h^+$  and  $\cdot\text{OH}$  were extremely active in the photocatalytic reaction that degraded RR2. To elucidate the photocatalytic mechanism, the active species were identified by adding different scavengers to the photocatalytic reaction. Fig. 10 shows the photocatalysis of RR2 by 0.25BBV in the presence of different scavengers. When EDTA-2Na and Cr(VI) were added, the efficiency of the photocatalytic

removal of RR2 fell greatly from 98% to 33% and 11%, respectively. The small reduction of efficiency upon the addition of IPA revealed that  $\cdot\text{OH}$  might not have been the predominant active species. EDTA-2Na ( $h^+$  scavenger) and Cr(VI) ( $\cdot\text{O}_2^-$  radical scavenger) clearly caused rapid deactivation of the 0.25BBV and retarded the photocatalysis, indicating that the photo-induced holes and  $\cdot\text{O}_2^-$  radicals were the predominant active species in this photocatalytic system. The strengths of their effects followed the order  $\cdot\text{O}_2^- > h^+ > \cdot\text{OH}$ .

Under Vis. irradiation, both Bi<sub>2</sub>O<sub>3</sub> and BiVO<sub>4</sub> can generate electron-hole pairs. Typically, the electrons and holes travel in opposite directions because they are in a formed space-charge region [1]. Before a heterojunction is formed between Bi<sub>2</sub>O<sub>3</sub> and BiVO<sub>4</sub>, electrons move from the CB of Bi<sub>2</sub>O<sub>3</sub> to the VB of BiVO<sub>4</sub> by overcoming the internal built-up electrical field, resulting in the combination of electrons in the CB of Bi<sub>2</sub>O<sub>3</sub> and of holes in the VB of BiVO<sub>4</sub>. Mao et al. [16] suggested that both Bi<sub>2</sub>O<sub>3</sub> and BiVO<sub>4</sub> can be excited under Vis. irradiation, and that the holes in the VB of Bi<sub>2</sub>O<sub>3</sub> and the electrons in the CB of BiVO<sub>4</sub> recombine directly in their interfacial region. The electrons in the CB of Bi<sub>2</sub>O<sub>3</sub> are captured by the surface-chemisorbed O<sub>2</sub> to yield  $\cdot\text{O}_2^-$ , and

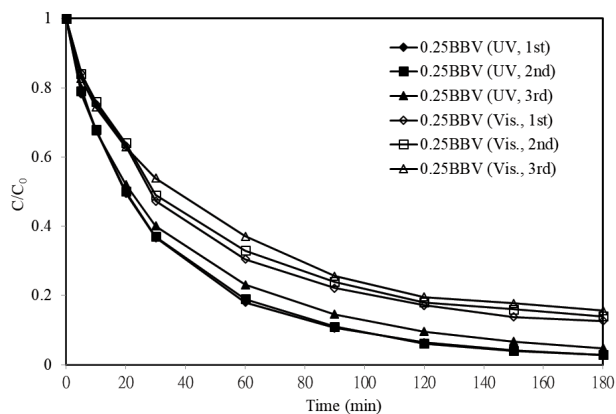


Fig. 9. Comparisons of cyclic photocatalysis of 0.25BBV under UV and Vis. irradiation ([RR2] = 20 mg/L, pH = 3, [photocatalyst] = 0.5 g/L).

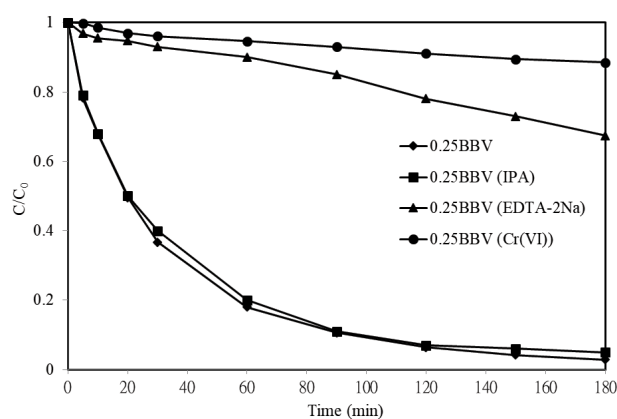


Fig. 10. Photocatalysis of RR2 by 0.25BBV in presence of different scavengers ([RR2] = 20 mg/L, pH = 3, [0.25BBV] = 0.5 g/L).

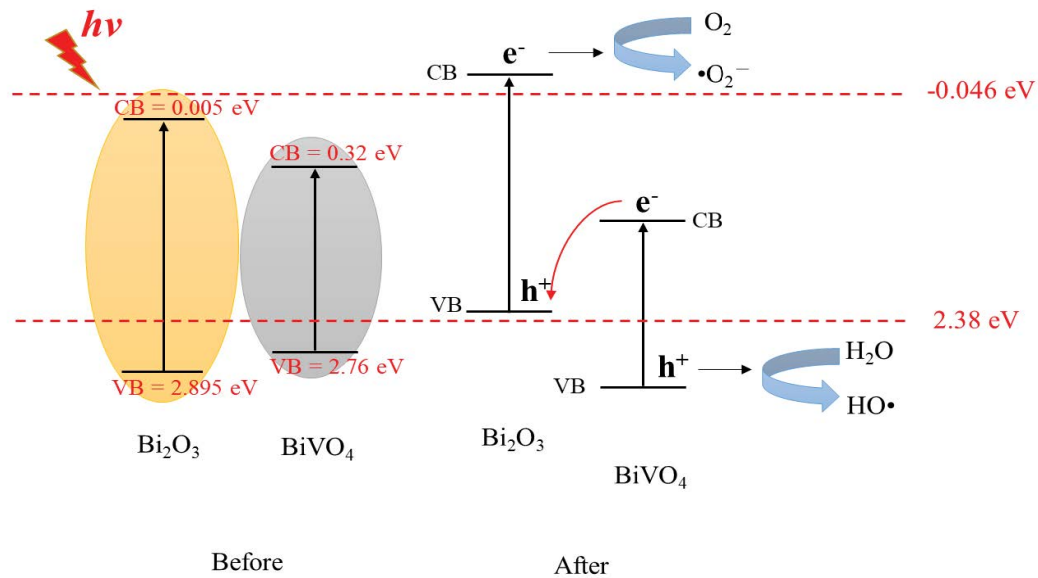


Fig. 11. Energy band diagram and possible charge-separation process of BBVs.

the remaining  $h^+$  in  $\text{BiVO}_4$  can directly oxidize organics.  $\text{Bi}_2\text{O}_3/\text{BiVO}_4$  is a category of direct Z-scheme photocatalysts, whose photocatalytic activity is greatly enhanced relative to those of  $\text{Bi}_2\text{O}_3$  and  $\text{BiVO}_4$  by the high charge transfer efficiency.

The corresponding CB and VB edge potentials are calculated using the following empirical equations [1,15,33,37,38].

$$E_{\text{CB}} = X - E_e - 0.5 E_g \quad (1)$$

$$E_{\text{VB}} = E_{\text{CB}} + E_g \quad (2)$$

where  $X$  is the absolute electronegativity of the semiconductors, expressed as the geometric mean of the absolute electronegativities of the constituent atoms. The absolute electronegativity is defined as the arithmetic mean of the atomic electron affinity and the first ionization energy. The  $X$  values for  $\text{Bi}_2\text{O}_3$  and  $\text{BiVO}_4$  are 5.95 and 6.04 eV, respectively [15].  $E_e$  is the energy of free electrons on the hydrogen scale (4.5 eV);  $E_g$  is the bandgap of the semiconductor, and  $E_{\text{CB}}$  and  $E_{\text{VB}}$  are the CB and VB edge potentials, respectively [1]. The  $E_{\text{CB}}$  values of  $\text{Bi}_2\text{O}_3$  and  $\text{BiVO}_4$  are determined to be 0.005 and 0.32 eV relative to the NHE level, respectively. The  $E_{\text{VB}}$  values of  $\text{Bi}_2\text{O}_3$  and  $\text{BiVO}_4$  are obtained as 2.895 and 2.76 eV, respectively. Consistent with previous studies, the CB and VB edge potentials of  $\text{Bi}_2\text{O}_3$  are approximately 0.29 and 2.67 eV versus NHE, respectively [18,39,40], and those of the  $\text{BiVO}_4$  are approximately 0.31 and 2.77 eV versus NHE [15,18,32,33]. These band edge positions of  $\text{Bi}_2\text{O}_3$  and  $\text{BiVO}_4$  were their potentials before contact. Fig. 11 presents the energy band diagram and possible charge-separation process of BBVs.  $\text{Bi}_2\text{O}_3$  is an intrinsic  $p$ -type semiconductor with a high hole mobility, which can serve as an electron donor in a photocatalyst.  $\text{BiVO}_4$  is an intrinsic  $n$ -type semiconductor, and can act as an electron acceptor, providing a pathway for interfacial charge transfer. This difference between CB and VB potentials generates a potential difference across the

interface of two photocatalysts, establishing a heterojunction. When  $\text{Bi}_2\text{O}_3$  and  $\text{BiVO}_4$  are in contact, a  $p$ - $n$  heterojunction is formed in the interfacial phase [15,16,18,19]. As a result of charge redistribution, the CB and VB of  $\text{Bi}_2\text{O}_3$  lie above those of  $\text{BiVO}_4$ . After the  $p$ - $n$  heterojunction is formed, the photo-generated electrons in the CB of  $\text{BiVO}_4$  are transferred to the VB of  $\text{Bi}_2\text{O}_3$ . The efficient separation of photo-generated electrons and holes in the  $p$ - $n$  heterojunction may considerably inhibit the recombination of the photo-generated charge carriers and extend their lifetime. Since the CB edge potential of  $\text{Bi}_2\text{O}_3$  is more negative than those of  $\text{BiVO}_4$  and of  $\text{O}_2/\cdot\text{O}_2^-$  (-0.046 V/NHE) [41], the photo-induced electrons may be trapped by the absorbed  $\text{O}_2$ , producing  $\cdot\text{O}_2^-$  [18]. Since the VB potential of  $\text{BiVO}_4$  is more positive than the potential of  $\cdot\text{OH}/\text{H}_2\text{O}$  (2.38 V/NHE),  $h^+$  can trap  $\text{H}_2\text{O}$  and  $\text{OH}^-$  and oxidize them to  $\cdot\text{OH}$ . However, only a little of the absorbed  $\text{H}_2\text{O}$  and  $\text{OH}^-$  can be oxidized because most of the holes in the VB of  $\text{BiVO}_4$  directly oxidize RR2. The findings herein suggest that the major active oxidation species in the photocatalysis of BBV systems are  $\cdot\text{O}_2^-$  and  $h^+$ . BBVs suppress the recombination of electron-hole pairs and improve the photocatalytic activities of  $\text{Bi}_2\text{O}_3$  and  $\text{BiVO}_4$ .

Mao et al. [16] concluded that  $\cdot\text{O}_2^-$  and  $h^+$  are the dominant reactive species in the oxidative degradation of phenol in BBVs. Qiu et al. [17] revealed that both  $h^+$  and  $\cdot\text{OH}$  are the major reactive species that dominate the degradation of bisphenol-A in BBVs. Furthermore,  $\cdot\text{O}_2^-$  is generated in BBVs, and is mainly responsible for the mineralization of ortho-dichlorobenzene [18]. In this study and Sun et al. [18], the hydrothermal method was used to synthesize BBVs and, in both studies,  $\cdot\text{O}_2^-$  played the most important role in the photocatalytic reactions.

#### 4. Conclusions

In this study, the single-step hydrothermal method was used to prepare BBVs. The measured surface areas followed the order BBVs >  $\text{BiVO}_4$  >  $\text{Bi}_2\text{O}_3$  and the bandgaps followed

the order  $\text{Bi}_2\text{O}_3 > \text{BBVs} > \text{BiVO}_4$ . 0.25BBV exhibited the highest photocatalytic activity. The rates of photocatalyzed removal of RR2 by 0.25BBV followed the order  $\text{UV} > \text{Solar} > \text{Vis}$ . and  $\text{pH } 3 > \text{pH } 9$ . 0.25BBV had good reusability and did not undergo photo-corrosion under UV or Vis. irradiation. The enhanced photocatalytic activity of BBVs was primarily attributable to the  $\text{Bi}_2\text{O}_3/\text{BiVO}_4$  p-n heterojunction structure. The transfer of charges between  $\text{Bi}_2\text{O}_3$  and  $\text{BiVO}_4$  inhibited the recombination of photo-generated electrons and holes, resulting in higher photocatalytic activity than that of  $\text{Bi}_2\text{O}_3$  or  $\text{BiVO}_4$  alone. A study of the photocatalytic mechanism revealed that  $\cdot\text{O}_2^-$  and  $\text{h}^+$  were the main reactive species in the BBV photocatalytic systems herein.

### Acknowledgement

The authors would like to thank the Ministry of Science and Technology and National Kaohsiung University of Science and Technology, for financially supporting this research under Contract No. MOST 107-2221-E-992-001-MY2 and 107M01-1, respectively.

### References

- [1] Q. Shi, W. Zhao, L. Xie, J. Chen, M. Zhang, Y. Li, Enhanced visible-light driven photocatalytic mineralization of indoor toluene via a  $\text{BiVO}_4/\text{reduced graphene oxide}/\text{Bi}_2\text{O}_3$  all-solid-state Z-scheme system, *J. Alloys Compd.*, 662 (2016) 108–117.
- [2] A. Malathi, J. Madhavan, M. Ashokkumar, P. Arunachalam, A review on  $\text{BiVO}_4$  photocatalyst: activity enhancement methods for solar photocatalytic applications, *Appl. Catal., A*, 555 (2018) 47–74.
- [3] P.M. Rao, L.L. Cai, C. Liu, I.S. Cho, C.H. Lee, J.M. Weisse, P.D. Yang, X.L. Zheng, Simultaneously efficient light absorption and charge separation in  $\text{WO}_3/\text{BiVO}_4$  core/shell nanowire photoanode for photoelectrochemical water oxidation, *Nano Lett.*, 14 (2014) 1099–1105.
- [4] L. Li, B. Yan,  $\text{BiVO}_4/\text{Bi}_2\text{O}_3$  submicrometer sphere composite: microstructure and photocatalytic activity under visible-light irradiation, *J. Alloys Compd.*, 476 (2009) 624–628.
- [5] L. Zhang, G. Tann, S. Wei, H. Ren, A. Xia, Y. Luo, Microwave hydrothermal synthesis and photocatalytic properties of  $\text{TiO}_2/\text{BiVO}_4$  composite photocatalysts, *Ceram. Int.*, 39 (2013) 8597–8604.
- [6] N. Wetchakun, S. Chainet, S. Phanichphant, K. Wetchakun, Efficient photocatalytic degradation of methylene blue over  $\text{BiVO}_4/\text{TiO}_2$  nanocomposites, *Ceram. Int.*, 41 (2015) 5999–6004.
- [7] O. Monfort, T. Roch, M. Gregor, L. Satrapinsky, D. Raptis, P. Lianos, G. Plesch, Photooxidative properties of various  $\text{BiVO}_4/\text{TiO}_2$  layered composite films and study of their photocatalytic mechanism in pollutant degradation, *J. Environ. Chem. Eng.*, 5 (2017) 5143–5149.
- [8] W. Wang, X. Huang, S. Wu, Y. Zhou, L. Wang, H. Shi, Y. Liang, B. Zou, Preparation of p-n junction  $\text{Cu}_2\text{O}/\text{BiVO}_4$  heterogeneous nanostructures with enhanced visible-light photocatalytic activity, *Appl. Catal., B*, 134 (2013) 293–301.
- [9] S. Min, F. Wang, Z. Jin, J. Xu,  $\text{Cu}_2\text{O}$  nanoparticles decorated  $\text{BiVO}_4$  as an effective visible-light-driven p-n heterojunction photocatalyst for methylene blue degradation, *Superlattices Microstruct.*, 74 (2014) 294–307.
- [10] E. Aguilera-Ruiz, U.M. García-Pérez, M.D.L. Garza-Galván, P. Zambrano-Robledo, B. Bermúdez-Reyes, J. Peral, Efficiency of  $\text{Cu}_2\text{O}/\text{BiVO}_4$  particles prepared with a new soft procedure on the degradation of dyes under visible-light irradiation, *Appl. Surf. Sci.*, 328 (2015) 361–367.
- [11] S. Chaiwichian, B. Inceesungvorn, K. Wetchakun, S. Phanichphant, W. Kangwansupamonkon, N. Wetchakun, Highly efficient visible-light-induced photocatalytic activity of  $\text{Bi}_2\text{WO}_6/\text{BiVO}_4$  heterojunction photocatalysts, *Mater. Res. Bull.*, 54 (2014) 28–33.
- [12] Y. Geng, P. Zhang, S. Kuang, Fabrication and enhanced visible-light photocatalytic activities of  $\text{BiVO}_4/\text{Bi}_2\text{WO}_6$  composites, *RSC Adv.*, 4 (2014) 46054–46059.
- [13] P. Ju, P. Wang, B. Li, H. Fan, S. Ai, D. Zhang, Y. Wang, A novel calcined  $\text{Bi}_2\text{WO}_6/\text{BiVO}_4$  heterojunction photocatalyst with highly enhanced photocatalytic activity, *Chem. Eng. J.*, 236 (2014) 430–437.
- [14] L. Chen, D. Meng, X. Wu, A. Wang, J. Wang, M. Yu, Y. Liang, Enhanced visible light photocatalytic performances of self-assembled hierarchically structured  $\text{BiVO}_4/\text{Bi}_2\text{WO}_6$  heterojunction composites with different morphologies, *RSC Adv.*, 6 (2016) 52300–52309.
- [15] L. Chen, Q. Zhang, R. Huang, S. Yin, S. Luo, C.T. Au, Porous peanut-like  $\text{Bi}_2\text{O}_3\text{-BiVO}_4$  composites with heterojunctions: one-step synthesis and their photocatalytic properties, *Dalton Trans.*, 41 (2012) 9513–9518.
- [16] M. Mao, F. Chen, C. Zheng, J. Ning, Y. Zhong, Y. Hu, Facile synthesis of porous  $\text{Bi}_2\text{O}_3\text{-BiVO}_4$  p-n heterojunction composite microrods with highly efficient photocatalytic degradation of phenol, *J. Alloys Compd.*, 688 (2016) 1080–1087.
- [17] P. Qiu, B. Park, J. Choi, M. Cui, J. Kim, J. Khim,  $\text{BiVO}_4/\text{Bi}_2\text{O}_3$  heterojunction deposited on graphene for an enhanced visible-light photocatalytic activity, *J. Alloys Compd.*, 706 (2017) 7–15.
- [18] J. Sun, X. Li, Q. Zhao, M.O. Tade, S. Liu, Construction of p-n heterojunction b- $\text{Bi}_2\text{O}_3/\text{BiVO}_4$  nanocomposite with improved photoinduced charge transfer property and enhanced activity in degradation of ortho-dichlorobenzene, *Appl. Catal., B*, 219 (2017) 259–268.
- [19] Y. Lee, M. Cui, J. Choi, J. Kim, Y. Son, J. Khim, Degradation of polychlorinated dibenzo-p-dioxins and dibenzofurans in real-field soil by an integrated visible-light photocatalysis and solvent migration system with p-n heterojunction  $\text{BiVO}_4/\text{Bi}_2\text{O}_3$ , *J. Hazard. Mater.*, 344 (2018) 1116–1125.
- [20] A. Malathi, V. Vasanthakumar, P. Arunachalam, J. Madhavan, M.A. Ghanem, A low cost additive-free facile synthesis of  $\text{BiFeWO}_6/\text{BiVO}_4$  nanocomposite with enhanced visible-light induced photocatalytic activity, *J. Colloid Interface Sci.*, 506 (2017) 553–563.
- [21] S. Selvarajan, A. Suganthi, M. Rajarajan, K. Arunprasath, Highly efficient  $\text{BiVO}_4/\text{WO}_3$  nanocomposite towards superior photocatalytic performance, *Powder Technol.*, 307 (2017) 203–212.
- [22] U. Lamdab, K. Wetchakun, S. Phanichphant, W. Kangwansupamonkon, N. Wetchakun, In  $\text{VO}_4\text{-BiVO}_4$  composite films with enhanced visible light performance for photodegradation of methylene blue, *Catal. Today*, 278 (2016) 291–302.
- [23] C. Lai, M. Zhang, B. Li, D. Huang, G. Zeng, L. Qin, X. Liu, H. Yi, M. Cheng, L. Li, Z. Chen, L. Chen, Fabrication of  $\text{CuS}/\text{BiVO}_4$  (0 4 0) binary heterojunction photocatalysts with enhanced photocatalytic activity for Ciprofloxacin degradation and mechanism insight, *Chem. Eng. J.*, 358 (2019) 891–902.
- [24] D. Lv, D. Zhang, X. Pu, D. Kong, Z. Lu, X. Shao, H. Ma, J. Dou, One-pot combustion synthesis of  $\text{BiVO}_4/\text{BiOCl}$  composites with enhanced visible-light photocatalytic properties, *Sep. Purif. Technol.*, 174 (2017) 97–103.
- [25] L. Song, Y. Pang, Y. Zheng, C. Chen, L. Ge, Design, preparation and enhanced photocatalytic activity of porous  $\text{BiOCl}/\text{BiVO}_4$  microspheres via a coprecipitation-hydrothermal method, *J. Alloys Compd.*, 710 (2017) 375–382.
- [26] S. Balachandran, M. Swaminathan, Facile fabrication of heterostructured  $\text{Bi}_2\text{O}_3\text{-ZnO}$  photocatalyst and its enhanced photocatalytic activity, *J. Phys. Chem., C*, 116 (2012) 26306–26312.
- [27] K. Su, Z.H. Ai, L.Z. Zhang, Efficient visible light-driven photocatalytic degradation of pentachlorophenol with  $\text{Bi}_2\text{O}_3/\text{TiO}_2$ , *J. Phys. Chem. C*, 116 (2012) 17118–17123.
- [28] M. Šu, C. He, V.K. Sharma, M.A. Asi, D. Xia, X.Z. Li, H. Deng, Y. Xiong, Mesoporous zinc ferrite: synthesis, characterization, and photocatalytic activity with  $\text{H}_2\text{O}_2/\text{visible light}$ , *J. Hazard. Mater.*, 211–212 (2012) 95–103.
- [29] Y. Chen, S. Yang, K. Wang, L. Lou, Role of primary active species and  $\text{TiO}_2$  surface characteristic in UV-illuminated

- photodegradation of Acid Orange 7, *J. Photochem. Photobiol., A*, 172 (2005) 47–54.
- [30] M.S. Gui, W.D. Zhang, Q.X. Su, C.H. Chen, Preparation and visible light photocatalytic activity of  $\text{Bi}_2\text{O}_3/\text{Bi}_2\text{WO}_6$  heterojunction photocatalysts, *J. Solid State Chem.*, 184 (2011) 1977–1982.
- [31] H. Huang, K. Liu, K. Chen, Y. Zhang, Y. Zhang, S. Wang, Ce and F comodification on the crystal structure and enhanced photocatalytic activity of  $\text{Bi}_2\text{WO}_6$  photocatalyst under visible light irradiation, *J. Phys. Chem. C*, 118 (2014) 14379–14387.
- [32] Z. He, Y. Shi, C. Gao, L. Wen, J. Chen, S. Song,  $\text{BiOCl}/\text{BiVO}_4$  p–n heterojunction with enhanced photocatalytic activity under visible-light irradiation, *J. Phys. Chem. C*, 118 (2014) 389–398.
- [33] H. Li, Y. Sun, B. Cai, S. Gan, D. Han, L. Niu, T. Wu, Hierarchically Z-scheme photocatalyst of  $\text{Ag}@\text{AgCl}$  decorated on  $\text{BiVO}_4$  (0 4 0) with enhancing photoelectrochemical and photocatalytic performance, *Appl. Catal., B*, 170–171 (2015) 206–214.
- [34] J. Su, X. Zou, G.D. Li, X. Wei, C. Yan, Y.N. Wang, J. Zhao, L.J. Zhou, J.S. Chen, Macroporous  $\text{V}_2\text{O}_5$ - $\text{BiVO}_4$  composites: effect of heterojunction on the behavior of photogenerated charges, *J. Phys. Chem. C*, 115 (2011) 8064–8071.
- [35] X. Zhang, L.Z. Zhang, T.F. Xie, D.J. Wang, Low-temperature synthesis and high visible-light-induced photocatalytic activity of  $\text{BiOI}/\text{TiO}_2$  heterostructures, *J. Phys. Chem. C*, 113 (2009) 7371–7378.
- [36] X. Ding, K. Zhao, L. Zhang, Enhanced photocatalytic removal of sodium pentachlorophenate with self-doped  $\text{Bi}_2\text{WO}_6$  under visible light by generating more superoxide ions, *Environ. Sci. Technol.*, 48 (2014) 5823–5831.
- [37] Z.Q. Li, X.T. Chen, Z.L. Xue, Microwave-assisted synthesis and photocatalytic properties of flower-like  $\text{Bi}_2\text{WO}_6$  and  $\text{Bi}_2\text{O}_3$ - $\text{Bi}_2\text{WO}_6$  composite, *J. Colloid Interface Sci.*, 394 (2013) 69–77.
- [38] X. Meng, Z. Zhang, Bismuth-based photocatalytic semiconductors: Introduction, challenges and possible approaches, *J. Mol. Catal. A: Chem.*, 423 (2016) 533–549.
- [39] H. Fan, H. Li, B. Liu, Y. Lu, T. Xie, D. Wang, Photoinduced charge transfer properties and photocatalytic activity in  $\text{Bi}_2\text{O}_3/\text{BaTiO}_3$  composite photocatalyst, *ACS Appl. Mater. Interfaces*, 4 (2012) 4853–4857.
- [40] G. He, C. Xing, X. Xiao, R. Hu, X. Zuo, J. Nan, Facile synthesis of flower-like  $\text{Bi}_{12}\text{O}_{17}\text{C}_{12}/\beta\text{-Bi}_2\text{O}_3$  composites with enhanced visible light photocatalytic performance for the degradation of 4-tert-butylphenol, *Appl. Catal., B*, 170–171 (2015) 1–9.
- [41] N. Tian, H. Huang, Y. He, Y. Guo, T. Zhang, Y. Zhang, Mediator-free direct Z-scheme photocatalytic system:  $\text{BiVO}_4/g\text{-C}_3\text{N}_4$  organic-inorganic hybrid photocatalyst with highly efficient visible-light-induced photocatalytic activity, *Dalton Trans.*, 44 (2015) 4297–4307.